INDERSCIENCE PUBLISHERS
Linking academia, business and industry through research

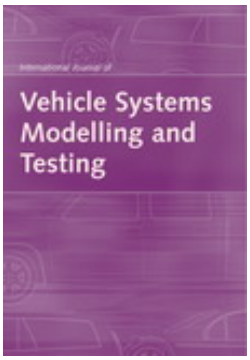

International Journal of Vehicle Systems Modelling and Testing

ISSN online: 1745-6444 - ISSN print: 1745-6436
https://www.inderscience.com/ijvsmt

Contact stiffness modelling and analysis of brake disc with rough geometrical topography and manufacturing deviation

Hehe Kang, Xiang Liu, Qiaolei Hu, Xuan Liu, Huali Han, Yongcheng Long, Haizhou Yuan

DOI: 10.1504/IJVSMT.2025.10069045

Article History:

Received:	16 October 2024
Last revised:	17 December 2024
Accepted:	25 December 2024
Published online:	04 April 2025

Contact stiffness modelling and analysis of brake disc with rough geometrical topography and manufacturing deviation

Hehe Kang

School of Mechanical and Electrical Engineering,
Zhoukou Normal University,
Zhoukou, 466001, China
Email: kanghh@zknu.edu.cn

Xiang Liu*

School of Automobile Engineering,
Guilin University of Aerospace Technology,
Guilin, 541004, China
Email: liuxiang@guat.edu.cn
*Corresponding author

Qiaolei Hu, Xuan Liu and Huali Han

School of Mechanical and Electrical Engineering,
Zhoukou Normal University,
Zhoukou, 466001, China
Email: hzauhuqiaolei@163.com
Email: zzgylx925@163.com
Email: hanhuali2016@163.com

Yongcheng Long

State Key Laboratory of Vehicle NVH and Safety Technology,
China Automotive Engineering Research Institute Co., Ltd.,
Chongqing, 401122, China
Email: 506175638@qq.com

Haizhou Yuan

School of Mechanical and Electrical Engineering,
Zhoukou Normal University,
Zhoukou, 466001, China
Email: 2134745495@qq.com

Abstract: Contact stiffness plays an important role in braking efficiency, braking squeal, and vibration response of brake system. However, randomness of manufacturing deviations caused in manufacturing process can lead to unsteadiness of the contact stiffness. To investigate the quantitative relationship between manufacturing tolerance and fluctuation of the contact stiffness, a contact stiffness model of brake disc is established through statistical rough contact theory and nonlinear stuck-slipped spring element, and then its effectiveness is validated by experimental data. Based on the model, a comprehensive analysis of various types of manufacturing deviations is conducted. The result shows that both normal and tangential initial contact stiffness are weakened by angular deviation and positively associated with positional deviation. This paper provides a novel way to reveal the inner mechanical relationship between macro-micro topography and initial contact stiffness of brake disc, which is significant for guiding tolerance design and performance optimisation of the brake system.

Keywords: manufacturing deviation; brake disc; rough interface; contact stiffness; normal contact; microscopic topography; stuck-slipped behaviour.

Reference to this paper should be made as follows: Kang, H., Liu, X., Hu, Q., Liu, X., Han, H., Long, Y. and Yuan, H. (2025) 'Contact stiffness modelling and analysis of brake disc with rough geometrical topography and manufacturing deviation', *Int. J. Vehicle Systems Modelling and Testing*, Vol. 19, No. 1, pp.47–73.

Biographical notes: Hehe Kang has a PhD in Mechanical Engineering and graduated from Shanghai Jiao Tong University in 2022. He is currently working at the School of Mechanical and Electrical Engineering, Zhoukou Normal University, Henan, China. His research interests include assembly analysis, rough contact, and dynamic modelling.

Xiang Liu received MEng in Vehicle Engineering from Hunan University in 2016. He is currently working at the School of Automotive Engineering, Guilin University of Aerospace Technology, Guangxi, China. His research focuses on structural design and automotive safety analysis.

Qiaolei Hu has a PhD in Agricultural Machinery Engineering and graduated from Huazhong Agricultural University in 2022. He is currently working at the School of Mechanical and Electrical Engineering, Zhoukou Normal University, Henan, China. His research interests include structural design, assembly analysis, and agricultural machinery.

Xuan Liu has a PhD in Mechanical Engineering and graduated from Northwestern Polytechnical University in 2022. He is currently working at the School of Mechanical and Electrical Engineering, Zhoukou Normal University, Henan, China. His research interests include gear transmission and geometrical deviation.

Huali Han has a PhD in Mechanical Engineering and graduated from Chongqing University in 2021. He is currently working at the School of Mechanical and Electrical Engineering, Zhoukou Normal University, Henan, China. Her research interests include surface friction and composite coating.

Yongcheng Long received MEng in Vehicle Engineering from Hunan University in 2016. He is a Senior Engineer and currently working at China Automotive Engineering Research Institute Co., Ltd., Chongqing, China. His research interests include vehicle NVH, structural crashworthiness and safety.

Haizhou Yuan is a sophomore at Zhoukou Normal University, majoring in Mechanical Design. He is quite interested in automobile braking safety and structural optimisation, and actively participates in relevant scientific research projects.

1 Introduction

Disc brake system is widely used in traffic vehicles due to its advantage in heat dissipation, light weight, and maintainability. As a core component, the disc brake system provides braking force for ensuring the normal operation condition of a whole vehicle (Vignati et al., 2021). However, braking process is a highly complex tribological phenomenon, potentially leading to various vibration and noise issues (Belhocine and Ghazaly, 2016; Belhocine and Abdullah, 2020; Thakre et al., 2022), which directly affects braking performance and the surrounding environment. To obtain a good braking performance of brake system, comprehensive parameter analysis has been conducted, such as the geometrical structure (Pan and Luo, 2024; Tyflopoulos et al., 2021; Kim et al., 2022; Stojanovic et al., 2023), the advanced material (Seo et al., 2021; Osenin et al., 2023; Sathyamoorthy et al., 2022), and the working condition (Chen et al., 2024; Kalhapure and Khairnar, 2021; Ishak et al., 2016; Vasiljevic et al., 2022). Considering that braking performance is almost determined by tangential contact behaviour of the brake disc, the friction characteristic analysis is regarded as an important foundational work in design and development of a brake system and has attracted much attention of researchers in the last years.

The brake system is usually subjected to severe loading conditions and a variety of external environments. It is challenging to analyse the friction behaviours of the brake component and the vibration noise caused by them. Quan et al. (2020) carried out an experiment to investigate the influence of shape parameters on friction noise, and the results showed that circular and triangular blocks can produce a low sound pressure. Zhang et al. (2024) analysed the stick-slip friction at a low brake speed and the transition phenomenon in vibration behaviour as the speed changes. The theoretical results indicated that the speed and contact stiffness can affect the stability of the vibration. Ehret et al. (2023) considered the deterministic and stochastic characteristics of the coefficient of friction and proposed an elaborate modelling method to predict braking distances. Yang et al. (2024) established a friction-induced vibration model to present the dynamic behaviour of an automotive brake system, and subsequently discussed the reliability of the brake system as well as the friction characteristics. Zhu et al. (2023) studied brake noise in railway disc under various brake conditions and found that the initial braking speed has a significant influence on brake squeal. In light of the aforementioned researches, it is clear that friction behaviour is very significant for vibration, noise, and braking performance of a brake system.

Considering that friction primarily involves the interaction of microscopic asperities on rough surfaces (Pinto et al., 2021; Xu et al., 2022; Zhang et al., 2022; Yang et al., 2023), it is necessary to delve into the contact characteristics on the brake system. Lai et al. (2020) proposed a finite element model to address the non-uniform contact at different

scales, and the results showed a strong dependency between the real contact area and vibration noise frequencies. Sha et al. (2022) considered the elastoplastic deformation of microscopic asperities in disc brakes and calculated wear life predications under different fractal geometrical parameters. Lee et al. (2013) analysed rough topography parameters and contact stiffness, finding that the tangential contact stiffness can affect the stuck-slipped amplitudes of disc brake. Pan et al. (2021) established a mathematical model of the brake system by introducing fractal contact stiffness and discussed the effect of fractal dimension and roughness on the nonlinearity of the system. Based on the present research, contact response is undoubtedly a crucial factor influencing braking performance, especially contact stiffness (Oh et al., 2005; Yoon et al., 2012; Magnier et al., 2014; Li et al., 2023). Hence, numerous studies have been conducted to investigate the contact stiffness of brake discs under various loading conditions (Ding et al., 2020; Ramasami et al., 2015; Yan et al., 2022).

However, contact stiffness is a complex physical characteristic that is associated with elastoplastic deformation, rough topography, and the material property of the contact surface. To better reveal the physical mechanism behind contact stiffness, Huang et al. (2024) established a contact model through fractal theory and studied the effect of fractal roughness on tangential stiffness. They found that a rougher surface tends to decrease the tangential stiffness. Pohrt and Popov (2013) studied the normal contact stiffness of a rigid indenter with randomly rough interface using the power spectrum method, and subsequently discussed the effect of topography wavelength on stiffness. Izmailov and Novoselova (2018) investigated the influence of the height distribution function and peak radius of asperity on contact stiffness. Gimpl et al. (2022) employed hysteresis loop measurements and substructuring techniques to obtain contact stiffness, and discussed the advantages and limitations of both methods. Additionally, considerable efforts have been made to enhance the effectiveness of theoretical models in presenting actual contact stiffness under various loading conditions and application fields (Li et al., 2023; Yu et al., 2021, 2022; Parel et al., 2020; Gao et al., 2024).

However, contact surfaces are rough and formed along with random manufacturing deviations in actual engineering (Shao et al., 2024; Ma et al., 2021, 2024). As these deviations are introduced, the tangential contact response of microscopic asperities inevitably changes, causing fluctuations in the slip ratio of the contact interface (Kang et al., 2021). In addition, the contact pressure deviates from the nominal design state, resulting in increased wear and a shorter service life for the mechanical system (Hjelm et al., 2021). Although contact stiffness has been extensively studied through both theoretical and experimental approaches, the influence of manufacturing deviations on contact stiffness remains unclear. Furthermore, existing contact stiffness models primarily focus on rough microscopic topography and neglect the coupling effect of macroscopic manufacturing deviations (Huang et al., 2024; Izmailov and Novoselova, 2018; Li et al., 2023; Yu et al., 2021, 2022; Parel et al., 2020; Gao et al., 2024). According to the currently published works, the internal relationship between manufacturing precision and discreteness of contact stiffness has not yet been revealed. Therefore, it is necessary to fill this gap in knowledge.

To build a bridge between manufacturing precision and the unsteadiness of contact stiffness, this paper attempts to propose a theoretical model to study the influence of manufacturing deviations on the initial contact stiffness of a brake disc. First, a normal

contact stiffness model is constructed, including elastoplastic deformation of microscopic asperities and macroscopic manufacturing deviations. By adopting IWAN model (Chen et al., 2024; Li and Zhang, 2024) to characterise the stuck-slipped behaviour of microscopic asperities, the tangential contact stiffness model is derived. Subsequently, the model is validated using experimental data. Through the theoretical model, the fluctuation and distribution of initial contact stiffness caused by manufacturing deviation are analysed in detail. The work presented in this paper provides significant guidance for manufacturing tolerance design and braking performance optimisation.

2 Contact modelling with manufacturing deviation

2.1 Description of manufacturing deviation

As shown in Figure 1, the disc and pad are the core components for brake system, since the friction behaviour between them provides the braking force for the entire vehicle (Patil and Khairnar, 2024). However, due to limited manufacturing precision in engineering, random geometrical and position deviations are inevitably generated in the brake system. To ensure good performance and assembly quality, the geometrical and the positional relationship between the brake disc and pad are generally specified to have a suitable dimensional and geometrical tolerances in the design phase.

Figure 1 Assembly structure of the brake system (see online version for colours)

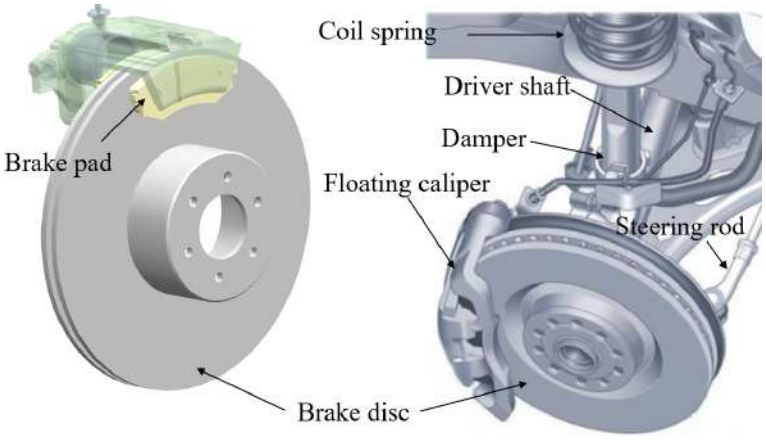

Figure 2 depicts the assembly and tolerance specifications of a typical brake disc and pad. The brake disc and pad are defined to be fully fixed and parallel to each other in the nominal geometrical and spatial state. The tolerance requirements about geometrical and positional precision of the brake disc and pad includes a parallelism tolerance of 0.01 mm, a perpendicularity tolerance of 0.01 mm, a radial runout tolerance of 0.025 mm, and a dimensional tolerance of ±0.01 mm. Specifically, the dimensional tolerance of ±0.02 mm for the brake pad is defined to restrict the positional deviation of its contact surface with respect to the brake disc. The parallelism tolerance of 0.01 mm and

perpendicularity tolerance of 0.01 mm are defined to restrict the angular deviation of the brake disc. By summing all related tolerance components in the translating and rotational directions respectively, the relative allowable geometrical tolerance zone of the contact interface can be obtained.

Figure 2 Tolerance specifications of the typical brake disc and pad: (a) tolerance and assembly structure of the floating calliper and (b) tolerance of the brake disc

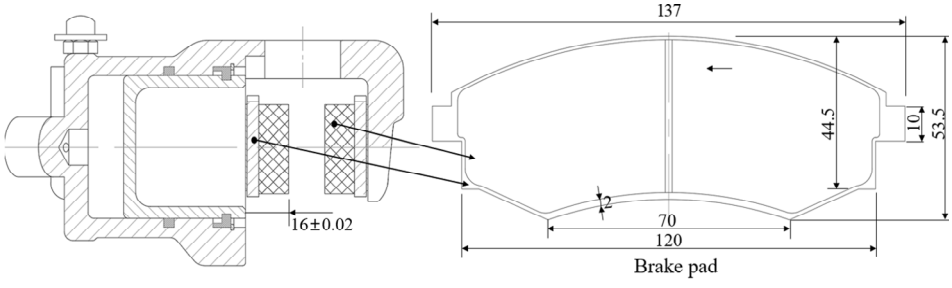

(a)

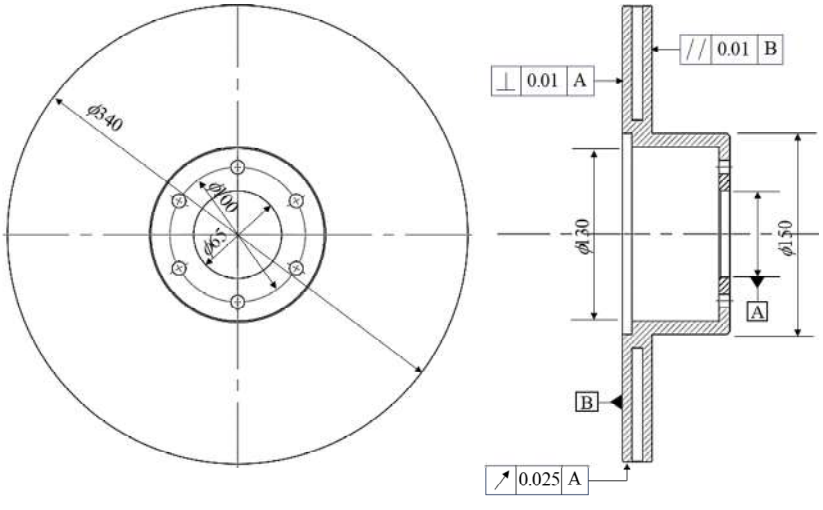

(b)

To facilitate theoretical modelling, the brake disc is assumed to have no manufacturing deviation, and the contact surface of the brake pad has an equivalent tolerance zone T with respect to the brake disc, as shown in Figure 3. S_n is the nominal surface, and S_v is the actual surface with random manufacturing deviation and allowed to vary randomly in the tolerance zone T. Based on small displacement torsor theory (Yang et al., 2023; Li et al., 2014), the actual manufacturing deviation of a plane can be characterised by a translational torsor δv along thickness direction, a rotational torsor $\delta\alpha$ along circumferential direction, and a rotational torsor $\delta\gamma$ along radial direction. Then, δv, $\delta\alpha$, and $\delta\gamma$ can be expressed as

$$\begin{aligned} -\frac{T}{2} \le \delta v \le \frac{T}{2} \\ -\frac{T}{b_{\max}} \le \delta\beta \le \frac{T}{b_{\max}} \\ -\frac{T}{L_{\max}} \le \delta\gamma \le \frac{T}{L_{\max}} \end{aligned} \tag{1}$$

where $L_{\max}$ and $b_{\max}$ are the maximum length and height of the brake pad and equal to 120 mm and 53.5 mm, respectively. T is the equivalent tolerance zone in the thickness direction of the brake pad and equal to 0.06 mm.

Figure 3 Tolerance zone of the brake pad with small displacement torsor (see online version for colours)

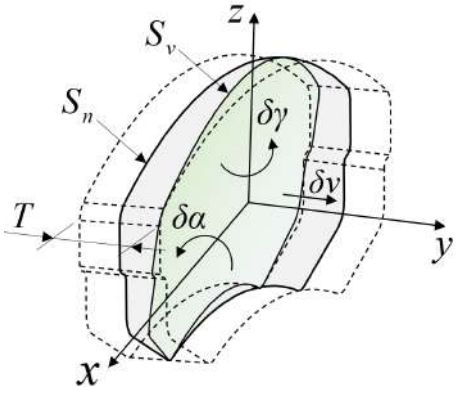

However, due to random manufacturing deviation, the actual contact state of brake interface deviates from the nominal state with the change of pressure distribution and tangential slip-stick behaviour. Accordingly, the contact stiffness is influenced, which can cause some serious functional problems, such as the braking noise, the reduction or lengthening of the brake distance, and the abnormal wear. In order to obtain good braking performance in actual engineering application, the contact stiffness of brake disc should be evaluated primarily with consideration of the geometrical and positional deviations.

2.2 Normal contact stiffness modelling

Contact stiffness depends on the contact behaviours of rough interface. According to GW contact theory (Zhao and Chang, 2001; Zhao et al., 2000; Brake, 2012), the general contact problem can be characterised by an equivalent rough surface and a rigid flat based. For the sake of modelling, several basic theoretical assumptions are made as follows: microscopic asperities have the same peak radius with random heights and do not interact with each other, and the roughness distribution is isotropic. As illustrated in Figure 4, z, ω, and R are the height, normal deformation, and peak radius of an asperity in contact, respectively. d_0 is the nominal separation distance between the rigid flat and the average level of the equivalent rough surface. It should be pointed out that the separation distance d is not a constant value and varies as the contact force and manufacturing deviation change. According to the description about the manufacturing deviation in

Figure 3, actual separation distance $d(x,z)$ can be characterised by the small displacement torsors (i.e., δv , $\delta\alpha$, $\delta\gamma$) and expressed as

$$d(x,z) = d_0 - \delta v + z\delta\alpha - x\delta\gamma \tag{2}$$

When normal contact force f is small, the contacting asperity only produce purely elastic deformation. The expression of the elastic contact force f_e and pressure p_e can be formulated by normal deformation ω as follows (Wang et al., 2017)

$$f_e = \frac{4}{3}ER^{1/2}\omega^{3/2}, p_e = \frac{4E}{3\pi}\left(\frac{\omega}{R}\right)^{1/2} \tag{3}$$

where Young's modulus E and Poisson's ratio v satisfy $1/E = \left(1-v_1^2\right)/E_1 + \left(1-v_2^2\right)/E_2$, and subscript 1 and 2 denote the two rough contact surfaces, respectively. As f increases, the asperity gradually comes into fully plastic deformation state, and the end point ω_1 for the purely elastic deformation is expressed as (Kogut and Etsion, 2002)

$$\omega_1 = R\left(\frac{\pi KH}{2E}\right)^{1/2} \tag{4}$$

where K is hardness coefficient and defined as $K = 0.454 + 0.41v$ (Xie et al., 2021; Eriten et al., 2011), and H stands for hardness of the softer one between two contacting materials. In the fully plastic state, the plastic contact force f_p and pressure p_p can be defined as (Zhao et al., 2000)

$$f_p = 2\pi HR\omega, p_p = H \tag{5}$$

The start point of the plastic deformation ω_2 is defined as $\omega_2 = 110\omega_1$ (Kogut and Etsion, 2002). For the transition phase ($\omega_1 < \omega < \omega_2$) between the purely elastic and fully plastic phases, the contacting asperity experiences mixed elastoplastic deformation, and the contact force f_{ep} can be constructed using an interpolation method. In order to obtain a smooth and continuous curve at the critical points between different deformation phases, elliptic function and logarithmic function are employed here, and f_{ep} can be expressed as (Kang et al., 2021)

$$\begin{aligned} f_{ep} &= p_{ep} \times a_{ep} \\ \frac{(\omega-\omega_2)^2}{C_1^{\,2}} &+ \frac{(p_{ep}-C_2)^2}{(p_2-C_2)^2} = 1 \\ a_{ep} &= R\pi\omega\left[1+3\left(\frac{\omega-\omega_1}{\omega_2-\omega_1}\right)^2 - 2\left(\frac{\omega-\omega_1}{\omega_2-\omega_1}\right)^3\right] \end{aligned} \tag{6}$$

where C_1 and C_2 are determined by the deformation continuity at the critical point ω_1 and ω_2. p_{ep} and a_{ep} are the contact pressure and area, respectively.

Based on equation (3)–(6), the formula of normal contact force f can be constructed in the whole deformation process. Considering that asperities are numerous in the rough surface, the height z is defined to obey Gaussian distribution as follows

$$\varphi^*(z^*)=\frac{\sigma}{\sqrt{2\pi}\sigma_s}\exp\left(-0.5\left(\frac{z^*\sigma}{\sigma_s}\right)^2\right) \tag{7}$$

where σ is standard deviation of the measured profile data, $z^*=z/\sigma$ is dimensionless height, η is asperity density, $\sigma_s/\sigma=\sqrt{1-3.717\times10^{-4}/\beta^2}$ (Eriten et al., 2011), and β is a roughness parameter and defined as $\beta=\eta\sigma R$. η, σ, and R depend on the actual rough profile and can be deduced through the spectral moment method (Eriten et al., 2011; Sun et al., 2019) as follows

$$\begin{cases} l_0=E[z^2] \\ l_2=E[(dz/dx)^2] \\ l_4=E[(d^2z/dx^2)^2] \end{cases} \Rightarrow \begin{cases} l_0^e=l_0^{c_1}+l_0^{c_2} \\ l_2^e=l_2^{c_1}+l_2^{c_2} \\ l_4^c=l_4^{c_1}+l_4^{c_2} \end{cases}$$
$$R=0.375\sqrt{\pi/l_4^e},\eta=l_4^e/\left(6\sqrt{3}\pi l_2^e\right),\sigma=\sqrt{l_0^e} \tag{8}$$

where $E[\ ]$ is expectation value, l_0, l_2, and l_4 denote different orders of spectral moments. c_1, c_2, and e indicate the two surfaces and the equivalent rough surface, respectively.

Figure 4 Equivalent contact of the rough interface (see online version for colours)

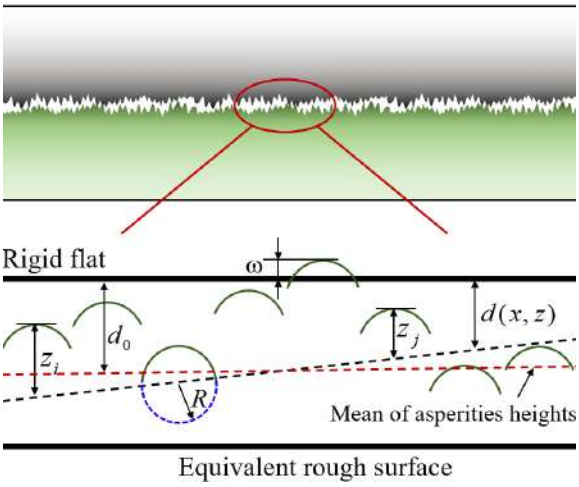

When $d(x,z)$ is determined, the normal resultant force N can be deduced as follows

$$N(d^*)=E\beta\times\left\{\begin{array}{l} \int\int_{d^*(x,z)}^{d^*(x,z)+\omega_1^*}\frac{4}{3}\left(\frac{\sigma}{R}\right)^{0.5}\omega^{*1.5}\varphi^*(z^*)\mathrm{d}z^*\mathrm{d}A \\ +\int\int_{d^*(x,z)+\omega_1^*}^{d^*(x,z)+\omega_2^*}\frac{a_{ep}^*p_{ep}^*}{RE\sigma}\varphi^*(z^*)\mathrm{d}z^*\mathrm{d}A \\ +\int\int_{d^*(x,z)+\omega_2^*}^{+\infty}2\pi\frac{H}{E}\omega^*\varphi^*(z^*)\mathrm{d}z^*\mathrm{d}A \end{array}\right\} \tag{9}$$

where A is the nominal contact area of the brake disc, and the symbol * indicates the normalised variables with respect to σ. From equation (9), it is clear that the normal contact resultant force N includes three components: the normal resultant force of asperities with elastic deformations, the resultant force with mixed elastoplastic deformation, and the force with fully plastic deformation. Based on the established normal contact model, the normal contact stiffness k_n can be deduced as the ratio of ΔN to Δd between the two surfaces, in which ΔN and Δd represent the fluctuations in N and d, respectively. Accordingly, stiffness k_n is expressed as

$$k_n = \frac{\Delta N(d)}{\Delta d} \tag{10}$$

2.3 Tangential contact stiffness modelling

Tangential response directly affects braking performance and should be thoroughly considered in structural design, performance optimisation, and manufacturing process. However, tangential contact is a complex phenomenon, including both stuck contact state and the slipped contact state. Compared with normal contact behaviour, characterising tangential contact response is more challenging, especially for rough interface coupled with macroscopic manufacturing deviations.

The Jenkins element of the IWAN model is adopted here to present the tangential response of contacting asperities, due to its good applicability to the nonlinear relationship between displacement and force (Ranjan and Pandey, 2021; Li et al., 2020). As shown in Figure 5, the Jenkins element is a nonlinear spring in which the spring force T_i increase linearly before stabilising at a constant value as the tangential displacement δ increases. Concretely, T_i can be defined as $T_i = \delta k$ under the small δ. However, T_i will reach its critical yield force q_i and then remain stable when δ is large enough. $T_i - \delta$ relationship of the Jenkins element can be expressed as (Chen et al., 2024)

$$T_i(\delta) = \begin{cases} k\delta, & 0 \le \delta \le q_i/k \\ q_i, & \delta \ge q_i/k \end{cases} \tag{11}$$

where k is the uniform stiffness coefficient. Accordingly, the linear deformation phase of the Jenkins element can be regarded as the tangential stuck contact of the asperity, while the stable phase represents the slipped contact of the asperity. By summing all tangential force T_i, the tangential resultant force T of the whole rough interface can be written as

$$T(\delta) = \sum_{j=1}^{F} q_j + \sum_{i=F+1}^{G} k_i \delta \tag{12}$$

where F is the number of slipped asperities, and G is total number of contacting asperities. It should be pointed out that the critical yield force q_i is not constant and determined by ω and z of the asperity. When G is large enough, T can be rewritten as follows (Li et al., 2020):

$$T(\delta) = \int_0^{k\delta} q\rho(q)\mathrm{d}q + k\delta\int_{k\delta}^{\infty} \rho(q)\mathrm{d}q \tag{13}$$

where $\rho(q)$ is the distribution function of the critical force q and directly deduced from the normal contact model in equation (19). Obviously, k in equation (13) is an undetermined mechanical parameter of the rough surface and difficult to be obtained

directly. For this reason, a normalisation method is employed herein to eliminate parameter k, and then $\rho(q)$, q, and δ in equation (13) are rewritten as (Segalman, 2005)

$$\begin{cases} \delta^* = \dfrac{\delta}{\sigma} \\ q = k\sigma\phi \\ \rho^*(\phi) = k^2\sigma^2\rho(q) \end{cases} \tag{14}$$

where ϕ, δ^* and $\rho^*(\phi)$ are dimensionless variables. Combining equations (14) and (13), T can be written as (Li et al., 2020)

$$T(\delta^*) = \int_0^{\delta^*} \phi\rho^*(\phi)\mathrm{d}\phi + \delta^* \int_{\delta^*}^{\infty} \rho^*(\phi)\mathrm{d}\phi \tag{15}$$

When δ^* approaches infinity, the second term will become infinitesimal, and all contacting asperities will be in slipped contact, indicating the occurrence of global slip in the whole interface. Accordingly, T will increase to its upper limit as

$$T_{\max}(\delta^*) = \int_0^{\infty} \phi\rho^*(\phi)\mathrm{d}\phi \tag{16}$$

For the global slip of the interface, the tangential force T is assumed to obey Coulomb law as

$$T_{\max} = \mu N \tag{17}$$

where μ is the friction coefficient. Combining equations (9) and (17), equation (16) can be rewritten as

$$\int_0^{+\infty} \phi\rho^*(\phi)d\phi = \mu E\beta \times \left\{ \begin{array}{l} \displaystyle\int\int_{d^*(x,z)}^{d^*(x,z)+\omega_1^*} \frac{4}{3}\left(\frac{\sigma}{R}\right)^{0.5} \omega^{*1.5}\varphi^*(z^*)\mathrm{d}z^*\mathrm{d}A \\ \displaystyle+\int\int_{d^*(x,z)+\omega_1^*}^{d^*(x,z)+\omega_2^*} \frac{a_{ep}^* p_{ep}^*}{RE\sigma}\varphi^*(z^*)\mathrm{d}z^*\mathrm{d}A \\ \displaystyle+\int\int_{d^*(x,z)+\omega_2^*}^{+\infty} 2\pi\frac{H}{E}\omega^*\varphi^*(z^*)\mathrm{d}z^*\mathrm{d}A \end{array} \right\} \tag{18}$$

Then, $\rho^*(\phi)$ can be deduced as

$$\rho^*(\phi,x,y) = \mu E\beta \times \begin{cases} \displaystyle\int \frac{4}{3}\left(\frac{\sigma}{R}\right)^{0.5} \phi^{0.5}\varphi^*(\phi + d^*(x,y))\mathrm{d}A & 0 \le \phi \le \omega_1^* \\ \displaystyle\int \frac{a_{ep}^* p_{ep}^*}{RE\sigma\phi}\varphi^*(\phi + d^*(x,y))\mathrm{d}A & , \quad \omega_1^* \le \phi \le \omega_2^* \\ \displaystyle\int 2\pi\frac{H}{E}\varphi^*(\phi + d^*(x,y))\mathrm{d}A & \omega_2^* \le \phi \end{cases} \tag{19}$$

Substituting equation (18) into equation (15), T can be constructed in a continuous and piecewise analytical form as follows:

$$T(\delta)=\begin{cases}\int_0^{\delta^*}\phi\rho^*\mathrm{d}\phi+\delta^*\int_{\delta^*}^{\phi_e}\rho^*\mathrm{d}\phi+\delta^*\int_{\phi_e}^{\phi_p}\rho^*\mathrm{d}\phi+\delta^*\int_{\phi_e}^{\infty}\rho^*\mathrm{d}\phi & 0\le\delta^*\le\omega_1^* \\ \int_0^{\phi_e}\phi\rho^*\mathrm{d}\phi+\int_{\phi_e}^{\delta^*}\phi\rho^*\mathrm{d}\phi+\delta^*\int_{\delta^*}^{\phi_p}\rho^*\mathrm{d}\phi+\delta^*\int_{\phi_p}^{\infty}\rho^*\mathrm{d}\phi & \omega_1^*\le\delta^*\le\omega_2^* \\ \int_0^{\phi_e}\phi\rho^*\mathrm{d}\phi+\int_{\phi_e}^{\phi_p}\phi\rho^*\mathrm{d}\phi+\int_{\phi_p}^{\delta^*}\phi\rho^*\mathrm{d}\phi+\delta^*\int_{\delta^*}^{\infty}\rho^*\mathrm{d}\phi & \omega_2^*\le\delta^*\end{cases} \tag{20}$$

In the presented tangential contact model, rough topography parameters and manufacturing deviations are introduced, and the tangential contact response of the interface with macro-micro topography can be obtained under a given normal contact force. Furthermore, the tangential contact stiffness k_t can be deduced from the ratio of the fluctuation ΔT of the tangential force T to the change $\Delta\delta$ of the tangential displacement δ. Accordingly, k_t can be written as

$$k_t=\frac{\Delta T(\delta)}{\Delta\delta} \tag{21}$$

Given the above analytical derivations, the normal and tangential contact stiffness models with macroscopic deviation and microscopic topography parameters are established. Correspondingly, a brief flow chart of the modelling process is given in Figure 6.

Figure 5 IWAN model on characterising stuck-slipped behaviour (see online version for colours)

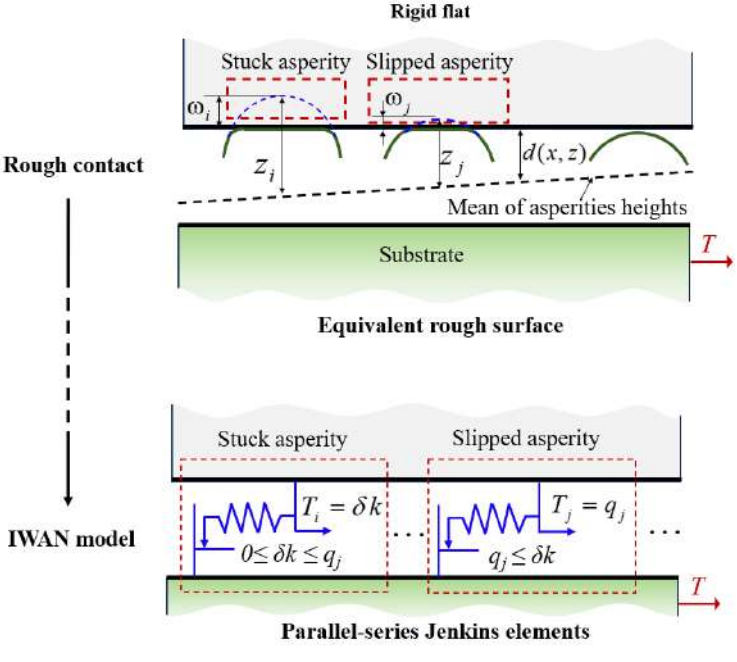

Figure 6 Flowchart for contact stiffness modelling with macro-micro topographies (see online version for colours)

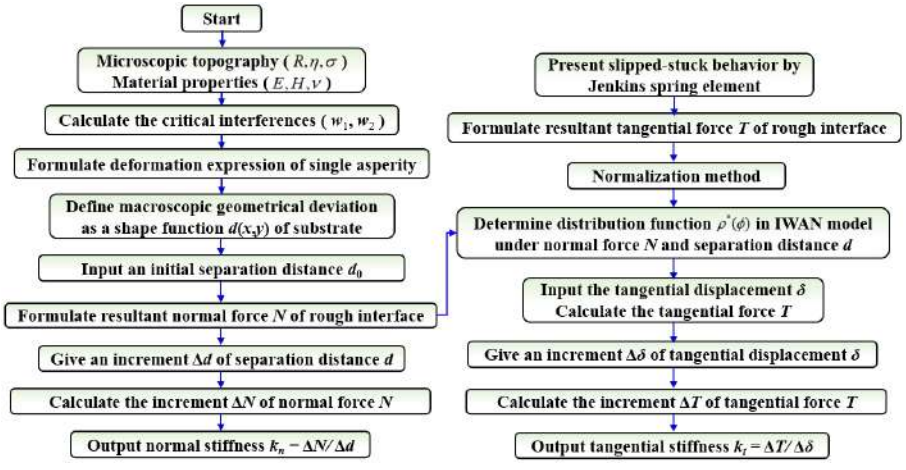

It should be pointed out that the contact stiffness of the brake disc is a resultant stiffness, calculated from the resultant normal and tangential contact force of the whole brake disc. The geometrical characteristics of the brake disc, namely its circular interface form and axisymmetric architecture, are not considered. The focus is mainly on the contact area A and macro-micro interface topography of the brake disc. On the other hand, the microscopic asperities in the rough interface undergo plastic deformation as the contact load is applied. After several applications of external loads, the geometrical parameters of the rough interface deviate from the initial topography, which causes the variation in the contact stiffness. Obviously, the actual rough topography parameters are not constant and vary during the braking process. However, it is difficult to measure the microscopic topography at any given time, especially in the working state. For this reason, the aforementioned contact stiffness modelling and calculation primarily focus on the initial geometrical topography, and the effect of topography variation caused by sliding conditions and braking process parameters is not taken into account here.

2.4 Model validation

The proposed contact model is validated herein via the comparison of hysteresis loops between the theoretical predictions and the experimental results (Eriten et al., 2011). The corresponding microscopic geometrical topography parameters and material properties are defined: $E = 106$ GPa, $H = 5.825$ GPa, $\nu = 0.24$, $\sigma = 2.677$ μm, $R = 30.14$ μm, $\eta = 2.91 \times 10^{-4}$ μm^{-2}, $A_0 = 170$ mm^2. By substituting the aforementioned parameters into the established contact stiffness model, the theoretical tangential force-displacement relationship can be calculated, which is then modified using Masing's function to generate the hysteresis curve. The corresponding Masing's function is defined as (Segalman, 2005).

$$\begin{cases} T_{\text{re}} = -T_{\max} + 2T\left(\dfrac{\delta_{\max} + \delta}{2}\right) & \dot{\delta} \geq 0 \quad \text{reloading} \\ T_{\text{un}} = T_{\max} - 2T\left(\dfrac{\delta_{\max} - \delta}{2}\right) & \dot{\delta} \leq 0 \quad \text{unloading} \end{cases} \tag{22}$$

Figure 7 depicts the hysteresis curves of the theoretical stiffness model and experiment (Eriten et al., 2011) under different bolt preloads. It can be found that all theoretical hysteresis curves of the tangential contact force T show strong agreement with the experimental results under $N = 234$ N, 331 N, 526 N, and 721 N, respectively. Thus, the proposed contact model is reliable and can be used in actual contact problem.

Figure 7 Hysteresis curves obtained from the theoretical and experimental results with different bolt preloads: (a) $N = 234$ N; (b) $N = 331$ N; (c) $N = 526$ N and (d) $N = 721$ N (see online version for colours)

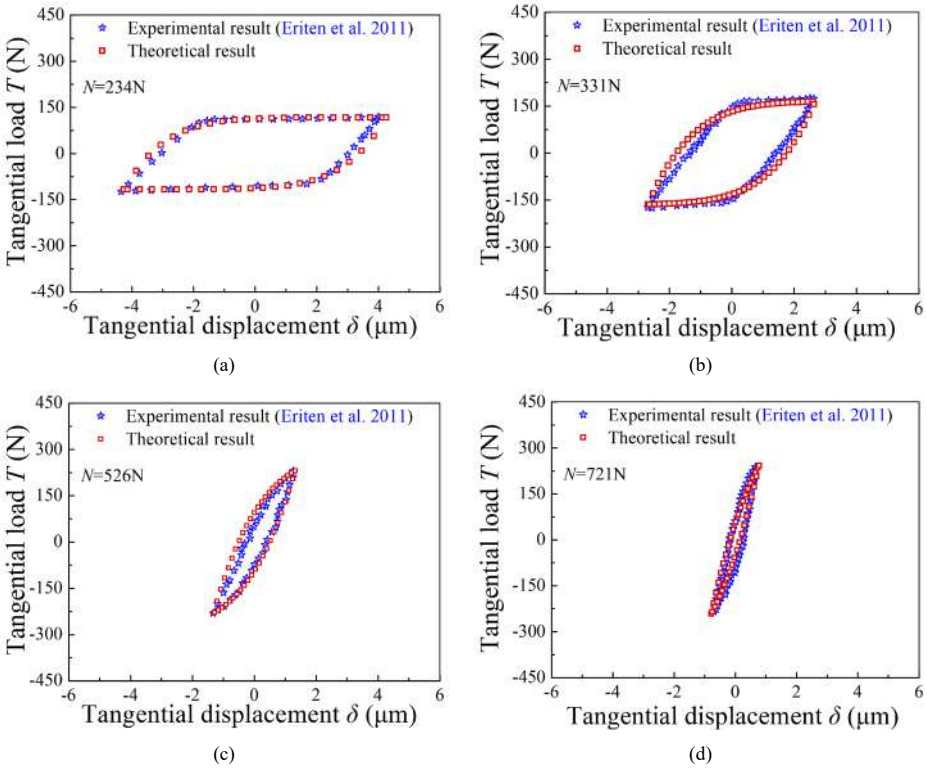

3 Parameter analysis

3.1 Rough topography parameter

The brake disc is made of G3500 grey iron with material parameters listed as: $E = 135$ GPa, $\nu = 0.27$, and $H = 2.49$ GPa. The nominal contact area of the brake disc is $A = 0.00469$ m^2. In order to conduct the following theoretical contact analysis, the actual

microscopic rough profile of brake disc is scanned using Keyence vk-x3000. In the measurement, the maximum height resolution is 0.01 nm, the sampling interval is approximately 1.384 μm, and the display resolution in the XY direction is 1 nm. The measurement repeatability accuracy in the XY direction is 50 nm. To obtain a comprehensive roughness distribution and eliminate the adverse effects caused by accidental machining errors, the height fields for three different random contact regions are measured, with a uniform sampling area of 1.415 × 1 mm. Figure 8 illustrates the 3D microscopic topographies of the rough surface in different samples measured by Keyence vk-x3000.

Figure 8 Microscopic rough topography of the brake disc measured by Keyence vk-x3000 (see online version for colours)

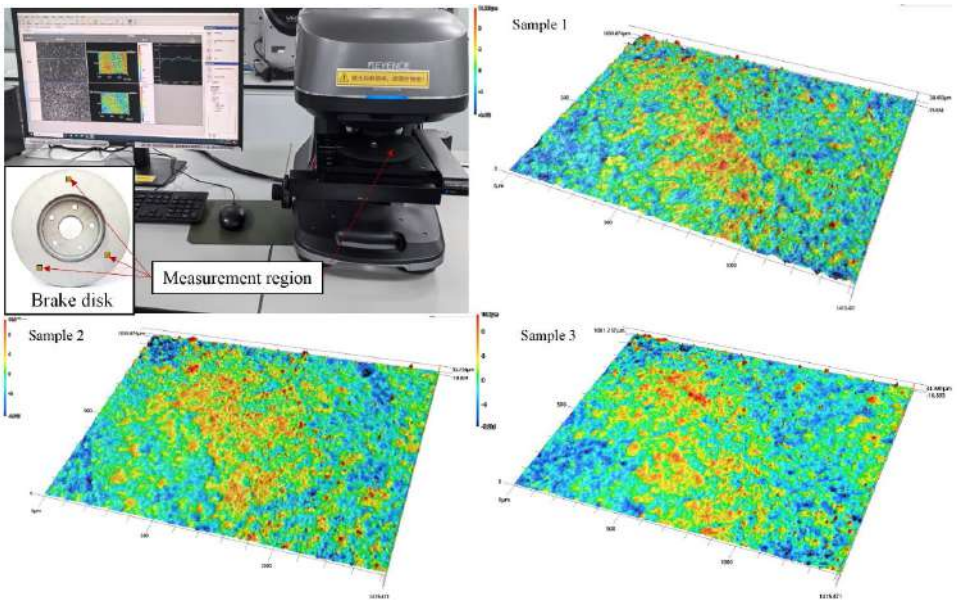

Considering that the locally heterogeneous distribution of the roughness and accidental scratches on the surfaces have a negative impact on characterising microscopic rough topography, four two-dimensional profiles for each measured region are extracted, as shown in Figure 9. Then, by substituting the height data into equation (8), the rough topography parameters are obtained and listed as follows: $R = 32.067$ μm, $\sigma = 3.034$ μm, and $\eta = 1.17 \times 10^9/\text{m}^2$. Furthermore, the contact stiffness analysis can be conducted through the proposed theoretical model. It should be pointed out that the abovementioned parameters are obtained under standard external environments (e.g., atmospheric temperature 25°). Although atmospheric temperature, reflection, and humidity may affect some parameters in the presented stiffness model, they are not considered here.

3.2 Effect of the angular deviation

The manufacturing deviation in the specified tolerance zone can be characterised via the translational and rotational torsors in the corresponding tolerance directions. Under the rotational torsors, the two contact surfaces have an angular deviation relative to each

other, which causes a change in the separation d between the two surfaces, as shown in equation (2) and Figure 4. Inevitably, the contact characteristics of the brake disc also vary due to the angular deviation. Figure 10 illustrates the normal contact stiffness of the brake disc under different angular deviations $\delta\alpha$ and $\delta\gamma$.

Figure 9 2D profile data of each measured region (Sample 1) (see online version for colours)

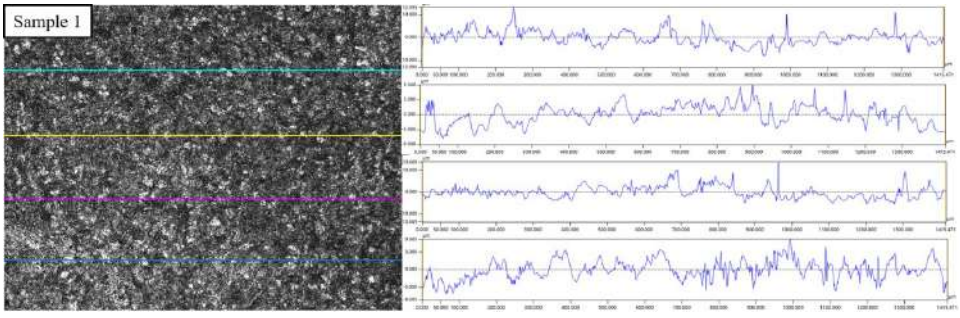

Figure 10 Normal contact stiffness of the brake disc under different angular deviation $\delta\alpha$ and $\delta\gamma$: (a) angular deviation $\delta\alpha$ and (b) angular deviation $\delta\gamma$ (see online version for colours)

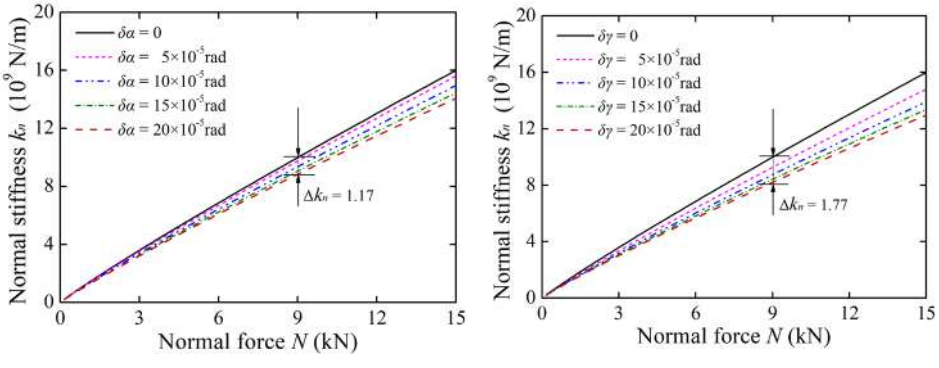

(a) (b)

It is observed that the normal contact stiffness k_n of the brake disc gradually increases with the normal force N generated by the hydraulic pressure from the brake calliper. This is mainly because, under large normal loads, more microscopic asperities come into contact and are more prone to plastic deformation compared to the smaller ones. Accordingly, the contact interface undergoes a greater alteration in normal force due to the growing number of contacting asperities and a higher degree of plastic deformations. Furthermore, it is clear that angular deviation can have a significant impact on k_n of the brake disc.

Specifically, as shown in Figure 10, k_n decreases as the angular deviation $\delta\alpha$ and $\delta\gamma$ increase from 0 to 20×10^{-5} rad. This indicates that angular deviation generated during the manufacturing process can weaken the normal contact between brake components and reduce braking effectiveness. It is also worth noting that the fluctuation $\Delta k_n = 1.77 \times 10^9$ N/m of k_n with angular deviation $\delta\gamma$ is larger than the fluctuation $\Delta k_n = 1.17 \times 10^9$ N/m with $\delta\alpha$ when normal force $N = 9$ kN. Obviously, the angular deviation $\delta\gamma$ has the stronger effect on the contact condition of brake disc than angular

deviation $\delta\alpha$. The main reason is that the length of the contact region (L_{max} = 120 mm) is greater than its width (b_{max} = 53.5 mm), and the maximum change Δd of the separation distance d caused by angular deviation $\delta\gamma$ is larger than that by the same angular deviation $\delta\alpha$. The contact region with larger Δd tends to generate more contacting asperities as well as plastic deformation.

Figure 11 illustrates the tangential contact stiffness k_t with different angular deviation. It is observed that k_t decreases as tangential force T increases. The reason is that the contact state of microscopic asperity is mainly in the stuck state for the small tangential force and it gradually transitions into the slipped state as the tangential force T increases. When T is large enough, the global sliding will occur at the contact interface and k_t comes to be zero. Similar to normal contact stiffness k_n, k_t is also affected by the angular deviation, since it decreases as $\delta\alpha$ and $\delta\gamma$ increase. Furthermore, it can also be seen that the fluctuation $\Delta k_t = 0.044 \times 10^9$ N/m of k_t caused by $\delta\gamma$ is larger than the stiffness fluctuation $\Delta k_t = 0.044 \times 10^9$ N/m caused by $\delta\alpha$ when normal contact force N = 1 kN and tangential force T = 0.1 kN. It means that the tangential contact stiffness is more responsive to changes in angular deviation $\delta\gamma$ than $\delta\alpha$. The same phenomenon can also be observed when subjected to different normal and tangential forces, for example, N = 5 kN and T = 0.6 kN.

Figure 11 Tangential contact stiffness of the brake disc under different angular deviation $\delta\alpha$ and $\delta\gamma$: (a) $\delta\alpha$ under N = 1 kN; (b) $\delta\gamma$ under N = 1 kN; (c) $\delta\alpha$ under N = 5 kN and (d) $\delta\gamma$ under N = 5 kN (see online version for colours)

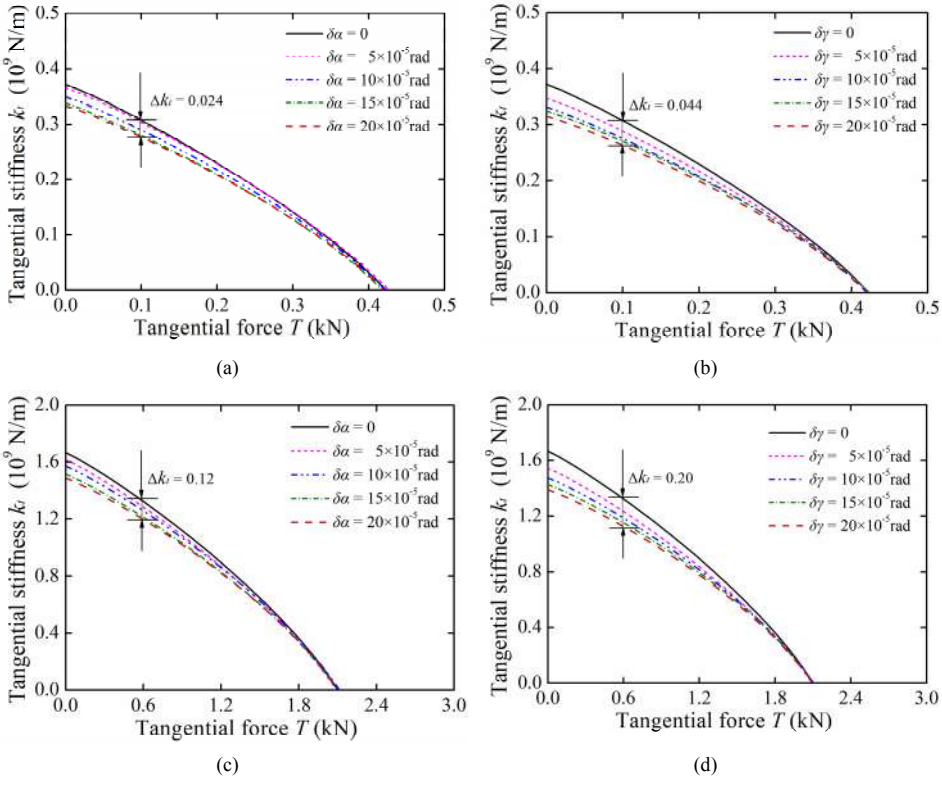

3.3 Effect of the positional deviation

The contact interface with positional deviation can be regarded as a translation with respect to the nominal position. Accordingly, the positional deviation is primarily related to brake pedal travel and braking distance during the braking process. In this section, the positional deviation is studied to show its influence on the normal and tangential contact stiffness for the given nominal separation d.

Figure 12 illustrates the normal contact stiffness of the brake disc when subjected to different positional deviations δv. It shows that the normal stiffness k_n decreases gradually as the separation d increases. The main reason is that the two contacting surfaces separate from each other as d increases, causing the microscopic asperities to produce more elastic deformations rather than plastic deformations. Meanwhile, the number of contacting asperities decreases as d increases. When d becomes large enough, global separation occurs at the contact interface, and k_n reaches zero. Besides, it can also be seen that k_n increases as positional deviation δv changes from –0.6 μm to 0.6 μm. When δv is positive value, the actual distance d is smaller than the nominal distance, consequently leading to an increase in the number of contacting microscopic asperities with plastic deformation. On the contrary, the negative δv leads to a larger distance d and reduction in the number of contacting microscopic asperities.

Figure 12 Normal contact stiffness of the brake disc under different positional deviation δv (see online version for colours)

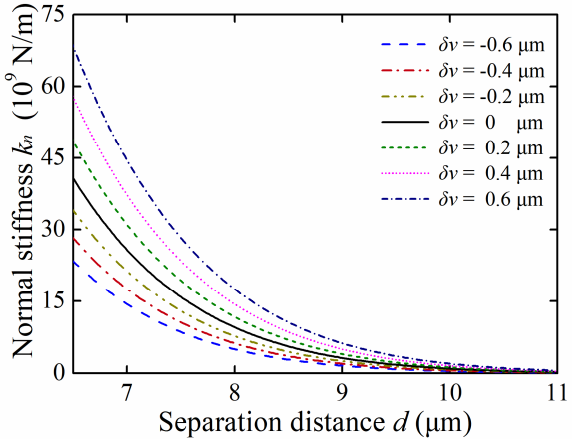

Figure 13 depicts the tangential contact stiffness k_t of the brake disc under different positional deviations δv when the separation distance $d = 9$ μm. It is clear that k_t decreases as the tangential displacement δ increases, and it nearly reaches zero when $\delta = 5$ μm, indicating that global slip occurs on the contact interface. Notably, the trend of change in k_t is similar to that of k_n as the positional deviation δv increases from –0.6 μm to 0.6 μm. The main reason is that a negative positional deviation δv reduce the number of contacting microscopic asperities, causing the asperities to be more prone to elastic deformation. As the positional deviation δv decreases, the normal contact force becomes smaller, and the contacting asperities tend to exhibit tangential slip, resulting in a small tangential force.

Figure 13 Tangential contact stiffness k_t of the brake disc under different positional deviation δv when separation distance d = 9 μm (see online version for colours)

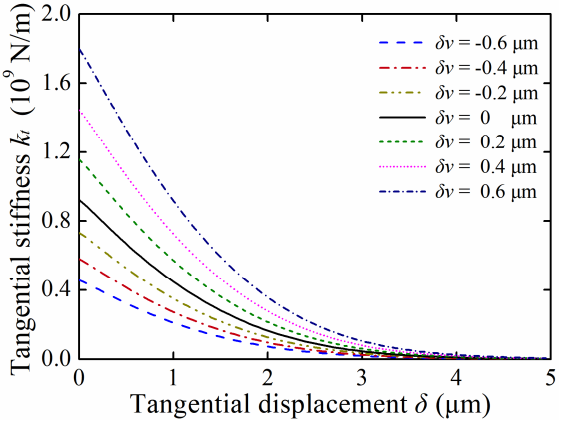

From the above results, it is known that the positional deviation can significantly affect both the normal and tangential contact stiffness for a given separation distance d. Considering that d is primarily related to the brake pedal travel, the positional deviation δv can weaken braking effectiveness and alter the brake pedal travel, which is extremely detrimental to vehicle safety.

3.4 Contact stiffness distribution under manufacturing tolerance

In actual surface, the positional and angular deviations generated during the manufacturing process are random within the allowed tolerance zone and usually follow a Gaussian distribution. To shed light on the relationship between manufacturing precision and the distribution range of contact stiffness, the fluctuations and distribution of contact stiffness caused by random manufacturing deviations are calculated. In this section, the tolerance zone of the contact interface is defined to be $T = 0.06$ mm, as shown in Figure 3. The positional and angular deviations are randomly produced within the tolerance zone T, as described in equation (1). However, the positional deviation δv and the angular deviations $\delta\alpha$ and δr are not independent of each other when considering the geometric constraint imposed by the tolerance boundary.

As illustrated in Figure 14, when the positional deviation δv and angular deviation $\delta\alpha$ reach their maximum, the actual surface will exceed the boundary of the tolerance zone T, which does not comply with the tolerance specification. For this reason, in addition to equation (1), the deviations δv, $\delta\alpha$ and δr must also satisfy the following constraint relationship

$$-\frac{T}{2} \le \delta v + \delta r \cdot x - \delta\alpha \cdot z \le \frac{T}{2} \tag{23}$$

To better present the statistical stiffness distribution under the given manufacturing tolerance $T = 0.06$ mm, 2000 samples of the deviations δv, $\delta\alpha$, and δr are generated randomly, with all deviations meeting the boundary constraint and Gaussian distribution. Figure 15 illustrates the distribution of δv, $\delta\alpha$, and δr. By substituting the above deviation samples into the presented theoretical model, the distribution and fluctuation of the

contact stiffness caused by manufacturing tolerance can be obtained, as illustrated in Figure 16. It is noted that k_t is calculated with a tangential displacement $\delta = 0.01$ μm here for numerical analysis. Clearly, the distribution and fluctuation of k_t with different δ can also be obtained using the presented method.

Figure 14 Boundary constraint of the tolerance zone (see online version for colours)

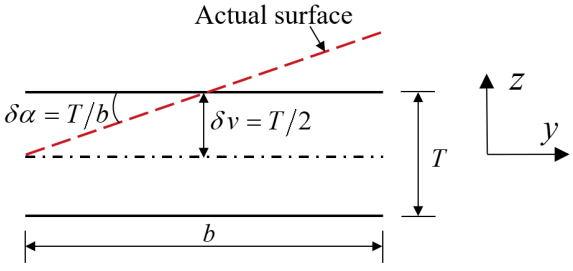

Figure 15 Distribution of manufacturing deviation under tolerance zone T: (a) positional deviation δv; (b) angular deviation $\delta\alpha$ and (c) angular deviation δr (see online version for colours)

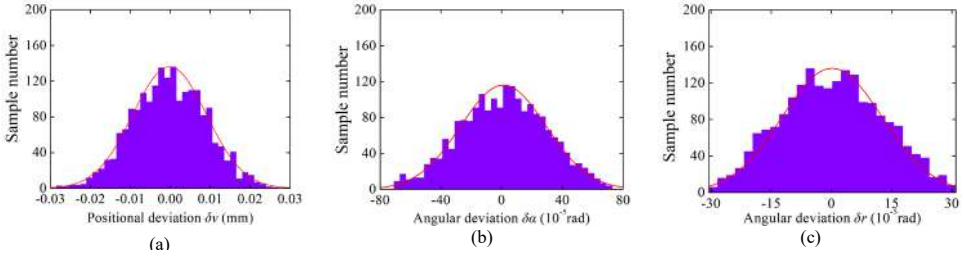

From Figure 16(a), it is observed that k_n and k_t are discretely distributed within a range that is determined by their respective upper and lower bounds. As normal force N varies from 0 kN to 15 kN, the fluctuation ranges of k_n and k_t gradually increase. Besides, the statistical distribution of k_n and k_t can be obtained when given a specified normal force N. Concretely, as shown in Figure 16(b)–(c), the distributions of k_n and k_t are approximatively the normal distribution, and the statistical distribution ranges ±3σ are [2.77, 4.49] and [1.29, 3.11], respectively.

Based on the presented results, the quantitative relationship between manufacturing tolerance and the statistical distribution of contact stiffness is established. This paper creatively proposes a methodology to bridge the gap between geometrical precision and the discrete interval of contact stiffness, which is novel and significant for guiding tolerance design and performance analysis of the brake system. However, some theoretical assumptions are made in this paper. For example, the geometrical simplification of microscopic asperities and the neglect of substrate deformation; the height of asperities follows Gaussian distribution; and the actual manufacturing deviation deviates linearly from the nominal surface. The above assumptions may adversely affect the effectiveness of the presented methodology in characterising the actual contact response of the brake disc.

Figure 16 Fluctuation and distribution of the contact stiffness caused by manufacturing tolerance T: (a) fluctuation range; (b) distribution of stiffness k_n for 5.5 kN < N < 6.5 kN and (c) distribution of stiffness k_t for 8.5 kN < N < 9.5 kN and δ = 0.01 μm (see online version for colours)

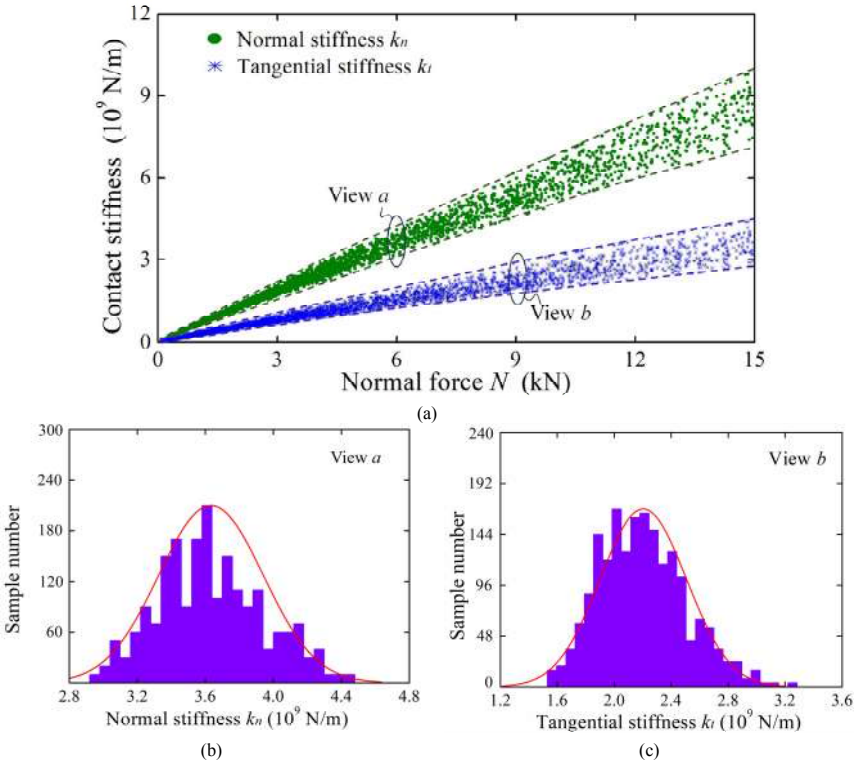

4 Conclusion

Contact stiffness is a crucial factor for the braking system, as it is directly related to braking efficiency, vibration, and noise. Due to manufacturing precision, the contact interface exhibits random macro-micro rough topography, which causes indeterminacy in contact stiffness in practical applications. To address this issue, this paper proposes a stiffness model to investigate the influence mechanism between macroscopic manufacturing deviation and contact stiffness of the brake disc. The model uses statistical rough contact theory and the Jenkins spring element to characterise the normal and tangential contact behaviour of microscopic asperities, and macroscopic manufacturing geometrical deviation is introduced as a linear shape function. Furthermore, a comparison is conducted to verify the efficacy of the proposed model. The effects of different types of manufacturing deviations are studied, and a quantitative relationship between initial contact stiffness and these deviations is established. The main conclusions are obtained as below:

- Compared with angular deviation $\delta\alpha$, angular deviation $\delta\gamma$ shows a stronger ability to reduce the initial contact stiffness and weaken braking effectiveness.

- Negative positional deviation δv, regarded as a reduction in the separation distance between the two contact surfaces, causes a noticeable increase in both normal and tangential contact stiffness.
- The fluctuation ranges of normal and tangential contact stiffness, caused by specified manufacturing tolerances, widen as the normal force increases.

The presented work provides significant guidance for manufacturing tolerance design. Additionally, it can also be used to investigate and diagnose vibration problems caused by manufacturing deviations. However, some theoretical assumptions are made in this paper, and the braking operation conditions and other mechanical parameters, such as the thermomechanical coupling effect, are not considered, which limits the effectiveness of the presented model in actual brake system. Therefore, more efforts should be made to improve this stiffness model in the future.

Acknowledgement

This work was supported by the Project of Science and Technology Tackling Key Problems in Henan Province of China (Nos. 242102221022, 242102111184, 242102220070), Natural Science Foundation of Henan Province (No: 242300420373), National College Student Innovation and Entrepreneurship Training Program of China (No:202410478016), and 2024 Guangxi University Young and Middle-aged Teachers' Basic Research Ability Improvement Project (No. 2024KY0812).

Conflict of interest

The author(s) declared no potential conflicts of interest with respect to the research, authorship, and/or publication of this paper.

References

Belhocine, A. and Abdullah, O.I. (2020) 'A thermomechanical model for the analysis of disc brake using the finite element method in frictional contact', *Journal of Thermal Stresses*, Vol. 43, No. 3, pp.305–320.

Belhocine, A. and Ghazaly, N.G. (2016) 'Effects of young's modulus on disc brake squeal using finite element analysis', *International Journal of Acoustics and Vibration*, Vol. 21, No. 3, pp.292–300.

Brake, M.R. (2012) 'An analytical elastic-perfectly plastic contact model', *International Journal of Solids and Structures*, Vol. 49, No. 22, pp.3129–3141.

Chen, H., Hao, Z.M., Kuang, J.X. and Mao, Y.J. (2024) 'Modeling of residual stiffness phenomenon in modified IWAN model of bolted joints and its application', *International Journal of Nonlinear Mechanics*, Vol. 167, p.104909.

Chen, X.T., Lu, C., Liu, X.Q., Sun, T.L. and Mo, J.L. (2024) 'The influence of competition between thermal expansion and braking parameter on the wear degradation of friction block', *Tribology International*, Vol. 192, p.109246.

Ding, H.Z., Zhu, Q. and Lyu, H.M. (2020) 'Identification of contact stiffness between brake disc and brake pads using modal frequency analysis', *Journal of Engineering and Technological Sciences*, Vol. 52, No. 4, pp.468–480.

Ehret, M., Hohmann, E. and Heckmann, A. (2023) 'On the modelling of the friction characteristics of railway vehicle brakes', *International Journal of Rail Transportation*, Vol. 11, No. 1, pp.50–68.

Eriten, M., Polycarpou, A.A. and Bergman, L.A. (2011) 'Physics-based modeling for fretting behavior of nominally flat rough surfaces', *International Journal of Solids and Structures*, Vol. 48, No. 10, pp.1436–1450.

Gao, Z.Q., Zhan, Y., Wei, X., Peng, L.X., Fu, W.P. and Wang, W. (2024) 'Study on normal contact stiffness characteristics in non-Gaussian rough surfaces under mixed lubrication', *Acta. Mechanica*, Vol. 235, pp.3535–3555.

Gimpl, V., Fantetti, A., Klaassen, S.W.B., Schwingshackl, C.W. and Rixen, D.J. (2022) 'Contact stiffness of jointed interfaces: a comparison of dynamic substructuring techniques with frictional hysteresis measurements', *Mechanical Systems and Signal Processing*, Vol. 171, p.108896.

Hjelm, R., Hansson, H., Ahadi, A., Andersson, C. and Wahlström, J. (2021) 'Influence of manufacturing error tolerances on contact pressure in gears', *Proceedings of the Institution of Mechanical Engineers, Part C: Journal of Mechanical Engineering Science*, Vol. 235, No. 20, pp.5173–5185.

Huang, G.C., Liu, C., Xie, W.Z. and Jiang, D.X. (2024) 'Tangential contact stiffness modeling between fractal rough surfaces with experimental validation', *Archive of Applied Mechanics*, Vol. 94, pp.719–736.

Ishak, M.R., Bakar, A.A., Belhocine, A., Taib, J.M. and Omar, W.Z.W. (2016) 'Brake torque analysis of fully mechanical parking brake system: theoretical and experimental approach', *Measurement*, Vol. 94, pp.487–497.

Izmailov, V.V. and Novoselova, M.V. (2018) 'Contact stiffness of machine components and the influence of the microgeometry of the contact surfaces on it', *Journal of Friction and Wear*, Vol. 39, pp.24–30.

Kalhapure, V.A. and Khairnar, H.P. (2021) 'Taguchi method optimization of operating parameters for automotive disc brake pad wear', *Applied Engineering Letters*, Vol. 6, No. 2, pp.47–53.

Kang, H.H., Li, Z.M., Liu, T., Zhao, G., Jing, J.P. and Yuan, W. (2021) 'A novel multiscale model for contact behavior analysis of rough surfaces with the statistical approach', *International Journal of Mechanical Sciences*, Vol. 212, p.106808.

Kim, S., Jwa, M., Lee, S., Park, S. and Kang, N. (2022) 'Deep learning-based inverse design for engineering systems: multidisciplinary design optimization of automotive brakes', *Structural and Multidisciplinary Optimization*, Vol. 65, No. 11, p.323.

Kogut, L. and Etsion, I. (2002) 'Elastic-plastic contact analysis of a sphere and a rigid flat', *Journal of Tribology-Transactions of the ASME*, Vol. 69, No. 5, pp.657–662.

Lai, V.V., Paszkiewicz, I., Brunel, J.F. and Dufrénoy, P. (2020) 'Multi-scale contact localization and dynamic instability related to brake squeal', *Lubricants*, Vol. 8, No. 4, p.43.

Lee, S.M., Shin, M.W., Lee, W.K. and Jang, H. (2013) 'The correlation between contact stiffness and stick–slip of brake friction materials', *Wear*, Vol. 302, pp.1414–1420.

Li, D.W., Botto, D., Xu, C. and Gola, M. (2020) 'A new approach for the determination of the IWAN density function in modeling friction contact', *International Journal of Mechanical Sciences*, Vol. 180, p.105671.

Li, H., Zhu, H.P., Li, P.G. and He, F. (2014) 'Tolerance analysis of mechanical assemblies based on small displacement torsor and deviation propagation theories', *The International Journal of Advanced Manufacturing Technology*, Vol. 72, pp.89–99.

Li, L., Sun, L.T., Wang, J.J., He, B.S., Fan, C.Q. and Li, L.X. (2023) 'Contact modeling and stiffness of a rough surface under mixed lubrication condition', *Journal of Mechanical Science and Technology*, Vol. 37, pp.851–864.

Li, W.B., Zhang, L.J., Zhang, C.M., Meng, D.J. and He, P.F. (2023) 'A study of the influence of heterogeneous friction coefficient and heterogeneous contact stiffness on the generation of squeal', *Proceedings of the Institution of Mechanical Engineers, Part D: Journal of Automobile Engineering*, Vol. 237, No. 9, pp.2143–2174.

Li, X. and Zhang, Z.S. (2024) 'Tangential contact modeling of joint interface considering elastic-plastic state based on IWAN model', *Tribology International*, Vol. 192, p.109238.

Ma, S.H., Hu, K.X., Hu, T.L. and Xiong, Z.Q. (2024) 'Two improved assembly deviation analysis methods based on Jacobian–torsor matrix and skin model shapes with contact deformation effort', *Proceedings of the Institution of Mechanical Engineers, Part B: Journal of Engineering Manufacture*, Vol. 238, pp.904–916.

Ma, S.H., Hu, T.L. and Xiong, Z.Q. (2021) 'Precision assembly simulation of skin model shapes accounting for contact deformation and geometric deviations for statistical tolerance analysis method', *International Journal of Precision Engineering and Manufacturing*, Vol. 22, pp.975–989.

Magnier, V., Brunel, J.F. and Dufrénoy, P. (2014) 'Impact of contact stiffness heterogeneities on friction-induced vibration', *International Journal of Solids and Structures*, Vol. 51, No. 9, pp.1662–1669.

Oh, J.E., Joe, Y.G. and Shin, K. (2005) 'Analysis of out-of-plane motion of a disc brake system using a two-degree-of-freedom model with contact stiffness', *Proceedings of the Institution of Mechanical Engineers, Part D: Journal of Automobile Engineering*, Vol. 219, No. 7, pp.869–879.

Osenin, Y.I., Krivosheya, D.S., Osenin, Y.Y. and Chesnokov, A.V. (2023) 'Disc brake design with carbon friction material', *Journal of Friction and Wear*, Vol. 44, pp.13–17.

Pan, G.Y. and Luo, X. (2024) 'Mechanism research and structure optimization of brake noise based on contact overlap degree', *Proceedings of the Institution of Mechanical Engineers, Part D: Journal of Automobile Engineering*, Vol. 238, No. 5, pp.1069–1080.

Pan, W.J., Ling, L.Y., Qu, H.Y. and Wang, M.H. (2021) 'Analysis of complex modal instability of a minimal friction self-excited vibration system from multiscale fractal surface topography', *European Journal of Mechanics – A/Solids*, Vol. 87, p.104226.

Parel, K.S., Paynter, R.J. and Nowell, D. (2020) 'Linear relationship of normal and tangential contact stiffness with load', *Proceedings of the Royal Society A-Mathematical Physical and Engineering Sciences*, Vol. 476, p.20200329.

Patil, L.N. and Khairnar, H.P. (2024) 'Assessing impact of smart brake blending to improve active safety control by using simulink', Applied Engineering Letters, Vol. 6, No. 1, 2021, pp.29–38.

Pinto, R.L.M., Gutiérrez, J.C.H., Pereira, R.B.D., Faria, P.E.D. and Rubio, J.C.C. (2021) 'Influence of contact plateaus characteristics formed on the surface of brake friction materials in braking performance through experimental tests', *Materials*, Vol. 14, No. 17, p.4931.

Pohrt, R. and Popov, V.L. (2013) 'Contact stiffness of randomly rough surfaces', *Scientific Reports*, Vol. 3, p.3293.

Quan, X., Mo, J.L., Huang, B., Tang, B., Ouyang, H.J. and Zhou, Z.R. (2020) 'Influence of the friction block shape and installation angle of high-speed train brakes on brake noise', *Journal of Tribology-Transactions of the ASME*, Vol. 142, p.031701.

Ramasami, D.N., Rejdych, G., Chancelier, T. and Pasquet, T. (2015) 'Stiffness distributions of brake pad friction materials using static and dynamic measurement techniques', *Proceedings of the Institution of Mechanical Engineers, Part D: Journal of Automobile Engineering*, Vol. 229, No. 6, pp.735–746.

Ranjan, P. and Pandey, A.K. (2021) 'Modeling of pinning phenomenon in IWAN model for bolted joint', *Tribology International*, Vol. 161, p.107071.

Sathyamoorthy, G., Vijay, R. and Lenin Singaravelu, D. (2022) 'Brake friction composite materials: a review on classifications and influences of friction materials in braking performance with characterizations', *Proceedings of the Institution of Mechanical Engineers, Part J: Journal of Engineering Tribology*, Vol. 236, pp.1674–1706.

Segalman, D.J. (2005) 'A four-parameter IWAN model for lap-type joints', *Journal of Applied Mechanics-Transactions of the ASME*, Vol. 72, No. 5, pp.752–760.

Seo, H., Park, J., Kim, Y.C., Lee, J.J. and Jang, H. (2021) 'Effect of disc materials on brake emission during moderate-temperature braking', *Tribology International*, Vol. 163, p.107185.

Sha, Z.H., Hao, Q., Yin, J., Ma, F.J., Liu, Y. and Zhang, S.F. (2022) 'Wear calculation and life prediction model of disc brake based on elastoplastic contact mechanics', *Advances in Mechanical Engineering*, Vol. 14, No. 4, pp.1–17.

Shao, N., Liu, J.H., Gong, H., Wang, R.L., Shi, S. and Anwer, N. (2024) 'An improved tolerance analysis method for gear mechanisms considering form deviations and elastic-plastic contact behaviors', *Precision Engineering*, Vol. 88, pp.742–758.

Stojanovic, N., Belhocine, A., Abdullah, O.I. and Grujic, I. (2023) 'The influence of the brake pad construction on noise formation, people's health and reduction measures', *Environmental Science and Pollution Research*, Vol. 30, pp.15352–15363.

Sun, Y.Y., Xiao, H.F. and Xu, J.W. (2019) 'Investigation into the interfacial stiffness ratio of stationary contacts between rough surfaces using an equivalent thin layer', *International Journal of Mechanical Sciences*, Vol. 163, p.105147.

Thakre, S., Shahare, A. and Awari, G.K. (2022) 'Investigation of thermal and structural response of disc brake of electric two wheeler for optimum performance', *International Journal of Vehicle Systems Modelling and Testing*, Vol. 16, No. 3, pp.240–258.

Tyflopoulos, E., Lien, M. and Steinert, M. (2021) 'Optimization of brake calipers using topology optimization for additive manufacturing', *Applied Sciences-Basel*, Vol. 11, No. 4, p.1437.

Vasiljevic, S., Glisovic, J., Stojanovic, B., Stojanovic, N. and Grujic, I. (2022) 'The analysis of the influential parameters that cause particles formation during the braking process: a review', *Proceedings of the Institution of Mechanical Engineers, Part J: Journal of Engineering Tribology*, Vol. 236, No. 1, pp.31–48.

Vignati, M., Canonico, G., Salustri, A.O., Sabbioni, E. and Tarsitano, D. (2021) 'Design and testing of a braking control logic for independently driven electric wheels', *International Journal of Vehicle Systems Modelling and Testing*, Vol. 15, Nos. 2–3, pp.81–101.

Wang, D., Xu, C. and Wang, Q. (2017) 'Modeling tangential contact of rough surfaces with elastic and plastic-deformed asperities', *Journal of Tribology-Transactions of the ASME*, Vol. 139, No. 5, p.051401.

Xie, W.Z., Liu, C., Jiang, D.X. and Jin, J.F. (2021) 'Inelastic contact behaviors of nanosized single-asperity and multi-asperity on α-Fe surface: molecular dynamic simulations', *International Journal of Mechanical Sciences*, Vol. 204, p.106569.

Xu, Y., Scheibert, J.L., Gadegaard, N. and Mulvihill, D.M. (2022) 'An asperity-based statistical model for the adhesive friction of elastic nominally flat rough contact interfaces', *Journal of the Mechanics and Physics of Solids*, Vol. 164, p.104878.

Yan, X.Y., Fan, C.L., Wang, W., Liu, X.J. and Chen, B.S. (2022) 'Study on the influence of radial stiffness on the nonlinear vibration of brake system', *Industrial Lubrication and Tribology*, Vol. 74, pp.10–17.

Yang, H.Y., Xu, C. and Guo, N. (2023) 'Modelling tangential friction considering contact pressure distribution of rough surfaces', *Mechanical Systems and Signal Processing*, Vol. 198, p.110406.

Yang, Z., Yuan, M.H., Yao, G. and Zhang, Y.M. (2024) 'Friction-induced vibration reliability and sensitivity analysis of a braking system', *Journal of Vibration and Control*, Vol. 01, pp.1–10.

Yang, Z.H., Yang, W.R., Gao, T.S. and Zhang, Y. (2022) 'Tolerance analysis method considering multifactor coupling based on the Jacobian–Torsor model', *Advances in Mechanical Engineering*, Vol. 14, No. 12, pp.1–13.

Yoon, S.W., Shin, M.W., Lee, W.G. and Jang, H. (2012) 'Effect of surface contact conditions on the stick–slip behavior of brake friction material', *Wear*, Vol. 294, pp.305–312.

Yu, X., Sun, Y.Y. and Wu, S.J. (2022) 'Multi-stage contact model between fractal rough surfaces based on multi-scale asperity deformation', *Applied Mathematical Modelling*, Vol. 109, pp.229–250.

Yu, X., Sun, Y.Y., Zhao, D. and Wu, S.J. (2021) 'A revised contact stiffness model of rough curved surfaces based on the length scale', *Tribology International*, Vol. 164, p.107206.

Zhang, Q.X., Yu, Z., Liu, H., Mo, J.L., Xiang, Z.Y., Zhu, S. and Jin, W.W. (2024) 'Analysis of friction-induced vibration and wear characteristics during high-speed train friction braking process', *Tribology International*, Vol. 196, pp.109701.

Zhang, S.Y., Li, D.W. and Liu, Y.W. (2022) 'Friction behavior of rough surfaces on the basis of contact mechanics: a review and prospects', *Micromachines*, Vol. 13, No. 11, p.1907.

Zhao, Y.W. and Chang, L. (2001) 'A model of asperity interactions in elastic-plastic contact of rough surfaces', *Journal of Tribology-Transactions of the ASME*, Vol. 123, No. 4, pp.857–864.

Zhao, Y.W., Maietta, D.M. and Chang, L. (2000) 'An asperity microcontact model incorporating the transition from elastic deformation to fully plastic flow', *Journal of Tribology-Transactions of the ASME*, Vol. 122, No. 1, pp.86–93.

Zhu, Q., Xie, J., Zhang, W., Chen, G.X. and Tuo, J.B. (2023) 'Effect of the braking parameter on disc brake squeal of a railway vehicle', *Wear*, Vol. 522, p.204884.

Nomenclature

S_n	Nominal surface with no deviation	T	Tolerance
S_v	Actual surface with geometrical deviation	$\delta\alpha$	Rotational torsor along circumferential direction
δv	Translational torsor along thickness direction	$\delta\gamma$	Rotational torsor along radial direction
L_{max}	Maximum length of brake pad	b_{max}	Maximum height of brake pad
z	Height of asperity	ω	Normal deformation of asperity
R	Peak radius of asperity	d_0	Nominal separation distance between two rough surfaces
f	Contact force of single asperity	f_e	Contact force in elastic phase
K	Hardness coefficient	f_p	Contact force in plastic phase
C_1, C_2	Constant coefficient	f_{ep}	Contact force in elastoplastic phase
σ	Standard deviation of rough profile	η	Asperity density
β	Roughness parameter	A	Nominal contact area
k_n	Normal contact stiffness	*	Normalised variable with respect to σ
N	Normal resultant force	l_0	Zero order of spectral moments
l_2	Second order of spectral moments	l_4	Fourth order of spectral moments
ΔN	Increment of normal resultant force	Δd	Increment of separation distance
T_i	Force of spring element	δ	Tangential displacement
k	Uniform stiffness coefficient of spring element	F	Number of slipped asperities
G	Total number of contacting asperities	q_i	Critical yield force of asperity

ϕ	Dimensionless tangential displacement	$\rho(q)$	Distribution function of the critical force q
μ	Friction coefficient	E	Young's modulus
T	Tangential resultant force	k_t	Tangential contact stiffness
ΔT	Increment of tangential force	$\Delta\delta$	Increment of tangential displacement